Title: Specificity, synergy, and mechanisms of splice-modifying drugs

Authors: Yuma Ishigami[1,*], Mandy S. Wong[1,†,*], Carlos Martí-Gómez[1], Andalus Ayaz[1], Mahdi Kooshkbaghi[1], Sonya Hanson[2], David M. McCandlish[1], Adrian R. Krainer[1,‡], Justin B. Kinney[1,‡].

Affiliations: 1. Cold Spring Harbor Laboratory, Cold Spring Harbor, NY, 11724, USA. 2. Flatiron Institute, New York, New York, 10010, USA.

Notes: [*]Equal contribution. [†]Present address: Beam Therapeutics, Cambridge, MA, 02142, USA. [‡]Correspondence: krainer@cshl.edu (ARK), jkinney@cshl.edu (JBK).

Abstract: Drugs that target pre-mRNA splicing hold great therapeutic potential, but the quantitative understanding of how these drugs work is limited. Here we introduce a biophysical-modeling framework that can quantitatively describe the sequence-specific and concentration-dependent behavior of splice-modifying drugs. Using massively parallel splicing assays, RNA-seq experiments, and precision dose-response curves, we apply this framework to two small-molecule drugs, risdiplam and branaplam, developed for treating spinal muscular atrophy. The results quantitatively define the specificities of risdiplam and branaplam for 5' splice site sequences, suggest that branaplam recognizes 5' splice sites via two distinct interaction modes, and disprove the prevailing two-site hypothesis for risdiplam activity at *SMN2* exon 7. The results also show, more generally, that single-drug cooperativity and multi-drug synergy are widespread among both small-molecule drugs and antisense-oligonucleotide drugs that promote exon inclusion. Our biophysical-modeling approach thus clarifies the mechanisms of existing splice-modifying treatments and provides a quantitative basis for the rational development of new therapies.

Introduction

Alternative pre-mRNA splicing has become a major focus of drug development[1–11]. The first splice-correcting drug approved by the US Food and Drug Administration was nusinersen (a.k.a. Spinraza™), an antisense oligonucleotide (ASO) developed to treat spinal muscular atrophy (SMA)[12–14]. Nusinersen functions by binding a complementary site in intron 7 of *SMN2* pre-mRNA, thereby blocking the RNA binding of a splicing repressor, hnRNPA1/A2, promoting the inclusion of *SMN2* exon 7, and rescuing full-length SMN protein expression. Because of its large size and negative charge, nusinersen does not efficiently cross the blood-brain barrier and is instead delivered intrathecally to cerebrospinal fluid[14].

A small-molecule drug, risdiplam (a.k.a. Evrysdi™ or RG7916; **Fig. 1A**), has also been approved for treating SMA[15–17]. Like nusinersen, risdiplam rescues *SMN2* exon 7 inclusion. Unlike nusinersen, risdiplam is able to cross the blood-brain barrier and can be delivered orally. Structural data has shown that risdiplam binds to and stabilizes the complex formed by 5' splice site (5'ss) RNA and the U1 snRNP at specific 5'ss sequences[18,19]. Still, the quantitative manner in which RNA sequence programs risdiplam activity has yet to be defined. Complicating matters, two studies have proposed that risdiplam further stimulates *SMN2* exon 7 inclusion by binding to a second RNA site within exon 7[18,20], and that the presence of this second RNA binding site substantially increases the specificity of risdiplam for *SMN2* exon 7 relative to all other 5'ss in the human transcriptome. This two-site hypothesis has become the prevailing explanation for risdiplam's pharmacological specificity[1,19,21–50]. However, the mechanism by which risdiplam recognizes this second RNA site remains unclear, as does the quantitative influence that this second RNA site has on the activation of *SMN2* exon 7 by risdiplam.

A second small-molecule drug, branaplam (a.k.a. NVS-SM1 or LMI070; **Fig. 1B**), also promotes the inclusion of *SMN2* exon 7 by targeting the U1/5'ss complex at specific 5'ss sequences[18,51,52]. Branaplam was originally developed to treat SMA, but appears to have more off-target effects than risdiplam[18,21] and is no longer being pursued for this indication[53]. In line with the two-site hypothesis for risdiplam, it has been proposed that the increased off-target behavior of branaplam relative to risdiplam is due, at least partly, to branaplam not binding to a second site within *SMN2* exon 7[18]. Fortuitously, one off-target effect of branaplam is the activation of a poison pseudoexon in the gene *HTT*. Because of this, branaplam has been proposed as a potential treatment for Huntington's disease[54–57]. A different off-target of branaplam, a pseudoexon in the gene *SF3B3*, has also

been repurposed as a chemically-inducible switch for gene therapies[25]. Still, the precise RNA-sequence determinants of branaplam activity have yet to be defined.

A major obstacle to defining the RNA specificities of risdiplam and branaplam, as well as the mechanistic basis for each drug's specificity, is the lack of mechanistically interpretable quantitative models for how splice-modifying drugs affect their targets. The lack of an established quantitative modeling framework for splice-modifying drugs contrasts with well-established equilibrium, quasi-equilibrium, and kinetic-modeling frameworks for protein-targeted drugs. Indeed, biophysical models for protein inhibitors and activators have existed for over a century[58,59], and are routinely used as a means of discerning drug mechanism[60]. The mechanistic complexity of splicing prevents the direct application of these established models to splice-modifying drugs. However, there remains the possibility that relatively simple "coarse-grained" biophysical models—ones that summarize the complex behavior of the spliceosome using a small number of parameters—might nevertheless be useful for quantifying the effects of splice-modifying drugs, as well as for illuminating the molecular mechanisms underlying these effects. Indeed, coarse-grained biophysical models have been proposed to describe how splicing is affected by genetic variation[61], but analogous models that describe how splicing is affected by splice-modifying drugs have yet to be developed.

Here we introduce a biophysical-modeling framework for splice-modifying drugs. We apply this framework to data from massively parallel splicing assays (MPSAs), RNA-seq experiments, and precision titration curves. The results quantitatively define the sequence-specificities of risdiplam and branaplam, change the mechanistic understanding of how these drugs function, and suggest novel strategies for developing therapeutics.

Results

MPSAs quantify the 5'ss-dependent effects of risdiplam and branaplam.

Previous studies showed that both risdiplam and branaplam bind to and stabilize the U1 snRNP / 5'ss complex at specific 5'ss sequences[18,19]. However, the sequence features required for U1/5'ss complex stabilization by either risdiplam or branaplam remain unclear. Other studies have reported position weight matrices (PWMs) for genomic 5'ss sequences that are activated by risdiplam or branaplam[25,51,54], but these PWMs convolve two fundamentally different signals: the sequence features that a 5'ss must have to be activated by drug, and the sequence features a 5'ss must have to be functional in the absence of drug. Understanding the mechanistic basis for 5'ss recognition by risdiplam and branaplam requires defining the 5'ss specificities of each drug in a manner that is not affected by drug-independent properties of the 5'ss sequence element.

To define the 5'ss specificities of risdiplam and branaplam, we used massively parallel splicing assays[62] (MPSAs) to measure the effects that risdiplam and branaplam have on variant 5'ss sequences in a fixed genetic context (**Fig. 1C**). We constructed a library of 285 three-exon minigenes (spanning exons 6, 7, and 8 of *SMN2*) in which all possible single-position and pairwise mutations were introduced at 8 positions of the exon 7 5'ss (agga/GUaagu, mutated positions in lowercase). This minigene library was transiently transfected into HeLa cells in the presence of risdiplam, branaplam, or solvent (DMSO, used as a negative control). The abundance of minigene mRNA including exon 7 relative to total minigene mRNA was then quantified using reverse transcription and high-throughput sequencing of barcodes present in different populations of isoforms. Positive and negative controls confirmed the ability of this MPSA to precisely measure percent spliced in (PSI) over a ~300× dynamic range (**Fig. S1**). The resulting PSI values are plotted in **Figs. 1D-I**.

MPSAs identify a motif for 5'ss activation by risdiplam.

We next sought to identify a motif that qualitatively describes which 5'ss in our minigene library were activated by risdiplam relative to DMSO. We formulated this motif-identification problem as a sequence-classification problem. Based on PSI measurements in the presence of risdiplam or DMSO, we categorized each of the 65,536 5'ss sequences of the form NNNN/GUNNNN into one of three classes: (class 1) 5'ss strongly activated by risdiplam; (class 2) 5'ss insensitive to risdiplam; or (class 3) 5'ss for which the effect of risdiplam could not be confidently determined, e.g., due to basal PSI being too high or too low, or the 5'ss not appearing in our minigene library; see **Supplemental Information** for details. We then searched for IUPAC motifs[63,64] that

matched all 5'ss in class 1 and did not match any 5'ss in class 2. The results show that multiple IUPAC motifs met these two criteria. These motifs differ in how many 5'ss in class 3 each one matches; these differences reflect uncertainties that result from the constrained nature of the sequence library and the finite dynamic range of the assay. We summarize this range of possible motifs with two specific motifs, the "ris min motif" and the "ris max motif". The ris min motif, ANGA/GUADGN, matches the minimal number of possible 5'ss (64 of 65,536) and thus defines an upper bound on risdiplam's specificity (**Fig. 1D**). The ris max motif, ANGA/GUHDNN, matches the maximal number of possible 5'ss (576 of 65,536) and thus defines a lower bound on risdiplam's specificity (**Fig. 1E**). We conclude that the ris min and ris max motifs accurately describe, for 5'ss in the *SMN2* minigene library, the sequence requirements for activation by risdiplam.

It is worth highlighting the sequence requirements for risdiplam activation identified by these IUPAC motifs. The ris min motif and ris max motif are identical in the exonic region (positions -4 to -1), and reveal that risdiplam activation requires A_{-4}, G_{-2}, and A_{-1}, but places no constraint on position -3 (see also **Fig. S2 A,B,C)**. The ris min and ris max motifs differ in the distal intronic region (positions +3 to +6), making the sequence requirements in this region more uncertain. Still, the ris max motif shows that, among the 5'ss sequence backgrounds assayed, risdiplam activity is abrogated by G_{+3} and by C_{+4}; this establishes that risdiplam does have specificity in the distal intronic region (see also **Fig. S2 D,E**).

MPSAs suggest a two-motif model for 5'ss activation by branaplam.

We next sought to identify a motif that qualitatively describes which 5'ss in our minigene library were activated by branaplam relative to DMSO. Based on PSI measurements in the presence of branaplam or DMSO, we categorized each 5'ss into one of three classes: (class 1) 5'ss strongly activated by branaplam; (class 2) 5'ss insensitive to branaplam; or (class 3) 5'ss for which the effect of branaplam could not be confidently determined. We then searched for IUPAC motifs that matched all 5'ss in class 1 and did not match any 5'ss in class 2. In contrast to risdiplam, the results show that no IUPAC motifs satisfy this branaplam activity classification criterion. This is evident from the fact that the minimally permissive IUPAC motif that matches all 5'ss in class 1 also matches some 5'ss in class 2 (**Fig. S3**). We conclude that the activity of branaplam, unlike the activity of risdiplam, cannot be accurately defined by a single IUPAC motif.

However, plotting PSI in the presence of branaplam versus risdiplam revealed that quantitative PSI measurements in these two conditions were remarkably similar (**Fig. 1F,G**). In particular, every 5'ss activated by risdiplam was also activated by branaplam, but a few 5'ss were activated substantially more by branaplam than by risdiplam. These observations are consistent with a "two-motif" model for branaplam, i.e., one in which branaplam recognizes two distinct but overlapping classes of 5'ss: 5'ss also activated by risdiplam, and 5'ss hyper-activated by branaplam relative to risdiplam.

We therefore sought to identify a motif that qualitatively describes which 5'ss in our minigene library were hyper-activated by branaplam relative to risdiplam. Based on PSI measurements in the presence of branaplam or risdiplam, we categorized each 5'ss into one of three classes: (class 1) 5'ss strongly hyper-activated by branaplam relative to risdiplam; (class 2) 5'ss with similar sensitivity to branaplam and risdiplam; or (class 3) 5'ss for which the comparative effects of risdiplam and branaplam could not be confidently determined. We then searched for IUPAC motifs that matched all 5'ss in class 1 and did not match any 5'ss in class 2. The results show that multiple IUPAC motifs satisfy these criteria. As with risdiplam activation, we summarize this range of possible motifs with two specific motifs, the "hyp min motif" and the "hyp max motif". The hyp min motif, RAGA/GURNGN, matches the minimal number of possible 5'ss (64 of 65,536) and thus defines an upper bound on the specificity of hyper-activation by branaplam (**Fig. 1F**). The hyp max motif, NANN/GUNNNN, matches the maximal number of possible 5'ss (16,384 of 65,536) and thus defines a lower bound on the specificity of hyper-activation by branaplam (**Fig. 1G**). Notably, the hyp max motif shows that hyper-activation by branaplam requires an A_{-3} (see also **Fig. S4**). We conclude that the hyp min and hyp max motifs accurately describe, for 5'ss in the *SMN2* minigene library, the sequence requirements for hyper-activation by branaplam relative to risdiplam.

Finally, we asked whether the two-motif model for branaplam accurately describes the set of 5'ss activated by branaplam relative to DMSO. Consistent with the two-motif model, the results show that every 5'ss activated by branaplam relative to DMSO matches both ris motifs and/or both hyp motifs. Moreover, every 5'ss insensitive

to branaplam relative to DMSO does not match either ris motif or either hyp motif (**Fig. 1H,I**). We conclude that the two-motif model accurately describes, for 5'ss in the *SMN2* minigene library, the sequence requirements for activation by branaplam.

MPSAs confirm and refine the 5'ss specificities of risdiplam and branaplam in a second gene context.

Having identified IUPAC motifs that describe the activities of risdiplam and branaplam at variant 5'ss in the context of *SMN2* exon 7, we investigated whether these motifs could predict drug effects in a different gene context. Using a previously reported[62] minigene library for *ELP1* exon 20 that contains nearly all 32,768 variant 5'ss of the form ANNN/GYNNNN, we performed MPSAs in the presence of risdiplam, branaplam, or DMSO. 5'ss that match the ris min motif were consistently activated by risdiplam relative to DMSO (**Fig. S5A)**, 5'ss that match the hyp min motif were consistently hyper-activated by branaplam relative to risdiplam (**Fig. S5B)**, and 5'ss that match either the ris min motif or the hyp min motif were consistently activated by branaplam relative to DMSO (**Fig. S5C**). The ris max motif performed nearly as well as the ris min motif, but yielded false-positive predictions for two 5'ss (**Fig. S5D**). The hyp max motif, by contrast, yielded many false positives (**Figs. S5E,F**). We conclude that, in the *ELP1* minigene context, the ris min motif accurately identifies 5'ss activated by risdiplam and by branaplam, and the hyp min motif accurately identifies 5'ss hyper-activated by branaplam relative to risdiplam.

RNA-seq confirms the 5'ss specificities of risdiplam and branaplam genome-wide.

Having identified IUPAC motifs that describe 5'ss activation by risdiplam and branaplam in two different minigene contexts, we next asked whether these IUPAC motifs could describe the effects of these drugs on cassette exons throughout the human transcriptome. Answering this question requires the ability to deconvolve the effects of 5'ss sequence on drug activity from the large exon-to-exon variability in basal PSI. However, no quantitative framework for distinguishing these effects has yet been described.

We therefore developed a coarse-grained biophysical model that separately accounts for genetic context and 5'ss-dependent drug effects (**Fig. 2A** and **Fig. S6**). This model makes three key assumptions: (1) PSI reflects the equilibrium occupancy of U1 on 5'ss RNA; (2) context strength, denoted by S, quantifies the stability of the U1/5'ss complex in the absence of drug (S depends on 5'ss sequence and on genetic context); (3) drug effect, denoted by E, quantifies how much a drug stabilizes or destabilizes the U1/5'ss complex (E depends on 5'ss sequence but not on genetic context). We describe this model as "coarse-grained" for two reasons. First, it reduces the complex kinetic cycle of the spliceosome to the initial U1/5'ss occupancy event, which is assumed to be in thermal equilibrium. Second, it aggregates the effects of 3' splice site (3'ss) sequence, branch point sequence, splicing regulatory proteins, etc., into a single quantity S. These simplifying assumptions are motivated by the established utility of similar models in studies of transcriptional regulation[65–70].

Our coarse-grained biophysical model allows genome-wide PSI measurements obtained in the presence and absence of drug to be quantitatively analyzed using a strategy previously developed for studying transcriptional regulation in bacteria[71]. Specifically, if one takes all exons in the genome that share a specific 5'ss sequence, and plots PSI in the presence of drug versus absence of drug for each of these exons, our model predicts the resulting plotted data points will approximately fall along a one-dimensional curve called an "allelic manifold" (**Fig. 2B**). The shape of this allelic manifold will reflect the quantitative value of drug effect, E, while the position of each data point along the allelic manifold will reflect the context strength, S, of the exon corresponding to that datapoint.

We used this coarse-grained biophysical model and allelic manifold analysis strategy to analyze RNA-seq data and thereby quantify 5'ss-dependent drug effects on exons throughout the human transcriptome (**Fig. 2C**). RNA-seq experiments were performed in HeLa cells treated with risdiplam, branaplam, or DMSO, and PSI values were determined for all identified internal exons (see **Methods**). Bayesian modeling of allelic manifolds was then used to infer drug-effect values for all 5'ss sequences of the form NNNN/GUNNNN that occur a sufficient number of times in the human transcriptome (see **Methods**). **Fig. 2D** shows the resulting drug-effect values determined for risdiplam and branaplam for the 2,521 distinct 5'ss sequences that satisfy these two criteria. **Fig. 2E** shows the allelic manifolds inferred for four specific 5'ss sequences. These inferred allelic manifolds explain the primary trends seen in our RNA-seq data, confirming that the 10-nt 5'ss sequence is a

major determinant of drug effect. We note, however, that some data points deviate significantly from their corresponding inferred allelic manifolds; this indicates that genetic context outside of the 10-nt 5'ss sequence has a detectable (if secondary) influence on drug effect. Understanding the mechanistic basis for this secondary influence on drug effect is a worthy goal for future research.

To validate the drug-effect values determined for risdiplam and branaplam, we asked whether these drug-effect values were consistent with known targets of these drugs. The 5'ss sequences of four exons known to be affected by risdiplam and/or branaplam are annotated in **Fig. 2D**; the corresponding allelic manifolds are shown in **Fig. 2E**. As expected, the effects of risdiplam and branaplam were nearly equal on the 5'ss sequence of *SMN2* exon 7, as well as on the alternative 5'ss of *FOXM1* exon 9, an established off-target for risdiplam that is believed to contribute to clinically relevant side effects[16]. Also as expected, branaplam had a strong effect (far stronger than risdiplam) on the 5'ss of *HTT* pseudoexon 50a, the target against which branaplam has been proposed as a potential treatment for Huntington's disease[54–57]. And again, as expected, branaplam had its strongest effect (far stronger than risdiplam) on the 5'ss of *SF3B3* pseudoexon 2a, the pseudoexon on which a branaplam-inducible gene therapy platform was recently developed[25]. We conclude that the drug-effect values determined for risdiplam and branaplam are consistent with important known targets of these two drugs.

We next investigated whether the drug-effect values determined for risdiplam and branaplam were consistent with the IUPAC motifs obtained from MPSA data. The results show that the ris min motif correctly identifies genomic 5'ss sequences strongly activated by risdiplam (**Fig. 2D**). By contrast, the hyp min motif misses many genomic 5'ss sequences that are activated by branaplam much more strongly than by risdiplam, and the hyp max motif matches many 5'ss that are not activated by branaplam much more strongly than by risdiplam (**Fig. S7**). Because the hyp min and hyp max motifs are, respectively, the most and least restrictive IUPAC motifs consistent with the MPSA data, we next examined the ability of IUPAC motifs with intermediate restrictiveness to explain the drug-effect values of branaplam relative to risdiplam. We found that the IUPAC motif NAGA/GURNGN (the "hyp min* motif") is the most restrictive motif that matches all genomic 5'ss sequences much more strongly activated by branaplam than risdiplam (**Fig. 2E**), while also being fully consistent with the MPSA data (**Fig. S8**). Note that the hyp min* motif is identical to the hyp min motif, except that it permits any base (rather than just A or G) at position -4. We conclude that the ris min motif accurately (though qualitatively) describes genomic 5'ss sequences strongly activated by risdiplam, and that the hyp min* motif accurately (though qualitatively) describes genomic 5'ss sequences much more strongly activated by branaplam than by risdiplam.

Biophysical modeling quantitatively defines the 5'ss specificities of risdiplam and branaplam.

Having established intuitive but qualitative descriptions of the 5'ss specificities of risdiplam and branaplam, we next sought to develop a biophysically interpretable quantitative model for these specificities. We therefore extended our coarse-grained biophysical model to reflect a specific hypothesized mechanism for how 5'ss sequence determines drug effect (**Fig. 3A; Fig. S9**). This model assumes that four distinct U1/5'ss complexes are possible, and that each complex has a "weight" that quantifies the occurrence frequency of that complex in thermal equilibrium. The four possible 5'ss/U1 complexes and their corresponding weights are: (1) a complex not bound by either drug (defined to have weight 1); (2) a complex bound by risdiplam (weight W_{ris}); (3) a complex bound by branaplam in a risdiplam-like interaction mode (also with weight W_{ris}); and (4) a complex bound by branaplam in a hyper-activation interaction mode (weight W_{hyp}). The logarithms of the weights W_{ris} and W_{hyp} are taken to be additive functions of 5'ss sequence. The quantitative "ris motif" comprises the additive parameters of $\log W_{\mathrm{ris}}$, and the quantitative "hyp motif" comprises the additive parameters of $\log W_{\mathrm{hyp}}$. We refer to this coarse-grained biophysical model as the "two-interaction-mode model for branaplam", as it formalizes the hypothesis that branaplam recognizes U1/5'ss in two distinct interaction modes (though the structural nature of these two hypothesized interaction modes remains undefined). For comparison, we developed an analogous "one-interaction-mode model for branaplam", which assumes that branaplam binds the U1/5'ss complex in a single interaction mode (**Fig. S10**). Importantly, the two-interaction-mode model for branaplam and one-interaction-mode model for branaplam have the same number of parameters.

We asked how well our data support the two-interaction-mode model for branaplam relative to the one-interaction-mode model for branaplam. Applying a Bayesian inference procedure to the PSI values measured

by MPSA, as well as to the drug-effect values measured by RNA-seq, we sampled parameter values from the posteriors of both models (see Methods). We then computed the log-likelihood of each set of parameters. The results show that the two-interaction-mode model for branaplam explains the MPSA and RNA-seq data much better than the one-interaction-mode model for branaplam does (**Fig. 3B**). Stratifying by dataset, the results show that the two-interaction-mode model for branaplam better accounts for the branaplam MPSA data and branaplam RNA-seq data, while similarly accounting for the risdiplam MPSA data, the DMSO MPSA data, and the risdiplam RNA-seq data (**Fig. S11**). Plotting these data against model predictions confirms that the two-interaction-mode model for branaplam explains these data for both drugs well (**Fig. 3C-F**) and better than the one-interaction-mode model for branaplam does (**Fig. S12**). We conclude that quantitative biophysical modeling supports the two-interaction-mode hypothesis for branaplam.

The ris motif and hyp motif obtained by this inference procedure (**Fig. 3G,H**) largely recapitulate the IUPAC motifs determined above. In the 5'ss exonic region, the ris motif and bran motif both show a prominent requirement for G_{-2} and A_{-1}. Moreover, the ris motif requires A_{-4} but is agnostic to the base at position -3, whereas the hyp motif requires A_{-3} but is agnostic to the base at -4. In the 5'ss intronic region, the ris motif strongly penalizes both G_{+3} and C_{+4}, behavior that is again consistent with the IUPAC ris min motif (**Fig. 1D,E**). Unlike the ris min motif or the hyp min* motif, neither the ris motif nor the hyp motif has a strong requirement for G_{+5}. However, the parameters of both motifs at this position remain highly uncertain. We conclude that our two-interaction-mode biophysical model describes the 5'ss specificities of both risdiplam and branaplam in a manner that is consistent with, but also refined relative to, the IUPAC motifs.

Risdiplam and branaplam exhibit specificity beyond that suggested by the bulge repair mechanism.

NMR structures of the U1 snRNA/5'ss mRNA complex in the presence and absence of SMN-C5 (an analog of risdiplam) led to the suggestion of a "bulge repair" mechanism for risdiplam activity[19]. In the absence of SMN-C5, the 5'ss A_{-1} bulges out of the minor groove of the U1 snRNA/5'ss double helix (**Fig. 4A**), destabilizing the helix and potentially clashing with U1-C, a protein component of the U1 snRNP. This A_{-1} bulge is caused by the 5'ss G_{-2} pairing in a shifted register with C_9 of the U1 snRNA. SMN-C5 binds within the dsRNA major groove, where its carbonyl group forms a hydrogen bond with the amino group of A_{-1}, thereby pulling the A_{-1} out of the minor groove and into the helical stack (**Fig. 4B**). This interaction stabilizes the RNA double helix by ~1 °C, and eliminates the potential clash with U1-C[19]. SMN-C5 is structurally similar to risdiplam (**Fig. 4C,D**), and is likely to stabilize the U1/5'ss complex by the same mechanism. Branaplam is less similar to SMN-C5 (**Fig. 4E**), but it possess a hydroxyl group and a pyridazine group in its center, and either of these groups might be positioned appropriately to form a hydrogen bond with the amino group of A_{-1}. Chemical shifts observed in a different NMR study[18] confirm the binding of branaplam to the U1 sRNA/5'ss mRNA complex in the vicinity of A_{-1}. These structural studies provide important context for interpreting our biophysical-modeling results.

Our biophysical-modeling results reveal specificity determinants beyond those suggested by the bulge-repair mechanism. The bulge-repair mechanism predicts a critical role for the $G_{-2}pA_{-1}$ dinucleotide. Consistent with this mechanism, both G_{-2} and A_{-1} are strongly required in both the ris motif and the hyp motif (**Figs. 3G,H**). However, the bulge-repair mechanism does not explain the strong hyp motif requirement for A_{-3} or the strong ris motif requirement for A_{-4}. Indeed, in the NMR structures of ref.[19], the 5'ss RNA fragment has a G at position -3 and does not extend to position -4. The bulge-repair mechanism also does not explain the preference, in both the ris motif and the hyp motif, for G > A > U > C at position +4. Low-throughput qPCR measurements (**Fig. 4G,H**) confirmed that both drugs prefer G > A > U > C at position +4 (as expected from **Fig. 3H**), and further revealed that both drugs prefer A > C, G, U at position +3 and G > A, C, U at position +5. We note that these observations of sequence specificity at positions +3, +4, and +5 are also consistent with chemical-shift data for branaplam and two risdiplam analogs reported by ref.[18]. We conclude that risdiplam and branaplam exhibit sequence specificity for the $G_{-2}pA_{-1}$ dinucleotide, consistent with the bulge-repair mechanism, but also exhibit additional specificity both upstream and downstream of the $G_{-2}pA_{-1}$ dinucleotide, specificity that is not explained by the bulge-repair mechanism.

We offer several potential and non-mutually-exclusive structural explanations for the two branaplam interaction modes suggested by our biophysical modeling results. One explanation is that branaplam has multiple tautomeric forms (**Fig. 4E**), and the different tautomeric forms of branaplam might bind the U1/5'ss complex in different orientations. A second explanation is that branaplam has two potential hydrogen-bonding groups in its

center (**Fig. 4E**, yellow highlight), and these could allow branaplam to interact with the A_{-1} in two different ways. A third explanation is that branaplam has more rotational degrees of freedom than risdiplam (**Fig. 4E**, green highlight), which could allow branaplam to adopt multiple conformations when interacting with the U1/5'ss complex. Molecular dynamics simulations confirmed that branaplam has greater conformational flexibility than risdiplam does (**Fig. S13**). A fourth explanation is that the approximate dihedral symmetry of dsRNA could facilitate the binding of risdiplam or branaplam in two flipped orientations, and that the sequence specificities of the two flipped orientations of branaplam are more distinct than are the sequence specificities of the two flipped orientations of risdiplam. Additional studies are needed to discern among these possible explanations.

Dose-response curves falsify the two-site hypothesis for risdiplam activity at* SMN2 *exon 7.

Our two-interaction-mode model for branaplam explains why risdiplam is more specific than branaplam at *SMN2* exon 7. Two publications[18,20] have proposed a different mechanism—the above-mentioned two-site hypothesis for risdiplam. In addition to one molecule of risdiplam stabilizing the U1/5'ss complex, this hypothesis states that a second molecule of risdiplam binds a purine tract (PT) within *SMN2* exon 7, thereby stabilizing a distinct protein-RNA complex that synergistically promotes exon inclusion (**Fig. 5A**). Distinguishing between these two competing hypotheses is essential for understanding the molecular mechanisms of risdiplam, branaplam, and splice-modifying small molecules more generally.

One prediction of the two-site hypothesis for risdiplam is that a molecule of risdiplam bound to the PT should promote *SMN2* exon 7 inclusion even when a second molecule of risdiplam is prevented from binding to the U1/5'ss complex. This prediction, however, is inconsistent with the observation, in our MPSA data, of risdiplam-insensitive 5'ss variants (i.e., the data points within the peach outlined area of **Fig. 1D,E**). These MPSA data therefore contradict the two-site hypothesis for risdiplam.

A second prediction of the two-site hypothesis for risdiplam is that disrupting the PT should reduce the cooperativity (i.e., Hill coefficient) of the response of *SMN2* exon 7 to risdiplam. To test this prediction, we used qPCR to obtain risdiplam dose-response curves for *SMN2* minigenes that carried either the wild-type PT or one of three previously reported PT disruptions: 25T26T (ref.[72]), Δ22-27 (ref.[20]), and Δ17-28 (ref.[18]); see **Fig. 5B**. We also extended our biophysical model from **Fig. 2A** to describe the concentration-dependent effects of splice-modifying drugs (**Fig. 5C,D**). This model has four parameters: (i) context strength of the target exon (S); (ii) maximal drug effect ($E_{\max}$); (iv) concentration of two-fold drug effect ($\mathrm{EC}_{2\mathrm{x}}$); and (iv) Hill coefficient (H); see **Fig. S14** for details. A Bayesian inference procedure was then used to infer values for these four parameters from each dose-response curve. Contrary to the two-site hypothesis for risdiplam, the results show that mutating the PT increased (rather than decreased) the Hill coefficient of risdiplam at *SMN2* exon 7 (**Fig. 5E-H**). Moreover, the risdiplam and branaplam Hill coefficients are statistically indistinguishable, regardless of whether or not the PT is present (**Fig. 5E-L**). We conclude that the dose-response data contradict the two-site hypothesis for risdiplam.

Our biophysical modeling results also provide an alternative explanation for data, reported in two prior studies[18,20], that were previously interpreted as supporting the two-site hypothesis for risdiplam. Both prior studies measured dose-response curves for risdiplam analogs (SMN-C3 and SMN-C5, respectively) in the context of *SMN2* minigenes having the wild-type PT or deletions in the PT (Δ17-28 and Δ22-27, respectively). Both prior studies observed that PT deletions increased EC_{50}, the drug concentration at which a PSI of 50 is achieved, and both prior studies interpreted this result as evidence for reduced cooperativity in the response to risdiplam analogs. Our biophysical model, however, highlights the fact that EC_{50} is affected by both cooperativity (quantified by H) and context strength (quantified by S). When applied to our dose-response data, this biophysical model reveals that PT mutations strongly reduce context strength while modestly increasing, not decreasing, cooperativity. This reduction in context strength fully accounts for the increases in EC_{50} that both prior studies observed when deleting the PT, and is consistent with the fact that the splicing activator Tra2-β1 is known[73] to bind the GGA sequence at positions 25-27 of exon 7. We propose that similar reductions in context strength likely account for the increase in EC_{50} observed by one of these prior studies[20] upon knocking down FUBP1 and KHSRP, two proteins that were proposed to bind the PT and mediate risdiplam-dependent splicing activation. We conclude that the prior observed effects of PT disruptions in cells is fully explained by the PT acting as a risdiplam-independent, rather than risdiplam-dependent, splicing enhancer.

We also conclude that biophysically interpretable quantitative models can play a valuable role in mechanistic studies of splice-modifying drugs.

Anomalous cooperativity is a common feature of splice-modifying drugs.

Our dose-response curves unexpectedly revealed that risdiplam and branaplam exhibit substantial cooperativity, i.e., have Hill coefficients greater than one. We refer to this phenomenon as "anomalous cooperativity" because it does not result from the simultaneous binding of multiple drug molecules. To understand if anomalous cooperativity occurs more generally, we investigated the dose-response behavior of other splice-modifying drugs.

We first asked if other drugs that promote the inclusion of *SMN2* exon 7 exhibit anomalous cooperativity. We measured dose-response curves for two antisense oligonucleotides, ASOi7 and ASOi6[12]. ASOi7 binds to *SMN2* intron 7 at positions +9 to +23 (relative to the 5'ss of exon 7), and presumably functions by the same mechanism as nusinersen. ASOi6 binds *SMN2* intron 6 at positions -55 to -41 (relative to the 3'ss of exon 7), and may function by blocking the RNA binding of the splicing repressor HuR[74]. The results show that ASOi7 exhibits anomalous cooperativity similar to risdiplam and branaplam (**Fig 6A**). The results also show that ASOi6 exhibits substantially less (if any) cooperativity (**Fig 6B**). These findings definitively establish that a splice-modifying drug can exhibit cooperativity even when it binds only a single site on target pre-mRNA, and that the extent of this cooperativity can differ between drugs that promote inclusion of the same cassette exon.

We then asked if splice-modifying drugs that promote the inclusion of exons other than *SMN2* exon 7 also exhibit anomalous cooperativity. We measured dose-response curves for two drugs, RECTAS and ASOi20, previously developed to treat familial dysautonomia. Both RECTAS and ASOi20 promote the inclusion of *ELP1* exon 20. RECTAS is a small molecule that is believed to function by indirectly enhancing the phosphorylation of the splicing factor SRSF6[75,76]. ASOi20 binds to *ELP1* intron 20 at positions +6 to +20 (relative to the 5'ss of exon 20), and functions through an unknown mechanism[77]. Our results show that RECTAS exhibits substantial cooperativity (**Fig 6C**), whereas ASOi20 exhibits less (if any) cooperativity (**Fig 6D**). We conclude that anomalous cooperativity is a common feature of splice-modifying drugs.

Multi-drug synergy is a common feature of splice-modifying drugs.

Even though the two-site hypothesis for risdiplam proved to be incorrect, we were motivated by this hypothesis to investigate whether two distinct drugs that promote inclusion of the same cassette exon, but which bind to distinct molecular targets, could synergistically promote exon inclusion. We therefore measured dose-response curves for various cocktails of splice-modifying drugs. The relative concentrations of the two drugs in each cocktail were chosen to be proportional to each drug's measured $\mathrm{EC}_{2\mathrm{x}}$ value (see **Supplemental Information**). For each cocktail, we then assessed the presence or absence of synergy based on whether the Hill coefficient of the drug mixture was larger than the Hill coefficients of the two individual drugs in the mixture. We note that many different tests of synergy have been proposed in the literature[78], and that we adopted this Hill coefficient test because it is simple, intuitive, and robust to experimental fluctuations in $\mathrm{EC}_{2\mathrm{x}}$ (we found $\mathrm{EC}_{2\mathrm{x}}$ to be highly sensitive to cell culture conditions). The results show no significant synergy for a risdiplam/branaplam cocktail at *SMN2* exon 7 (**Fig. 6E**). This observation is consistent with risdiplam and branaplam binding the same or overlapping sites in the *SMN2* exon 7 U1/5'ss complex. By contrast, the results show substantial synergy at *SMN2* exon 7 for a risdiplam/ASOi6 cocktail (**Fig. 6F**), a risdiplam/ASOi7 cocktail (**Fig. 6G**), and a branaplam/ASOi7 cocktail (**Fig. 6I**). The results also show strong synergy for a RECTAS/ASOi20 cocktail at *ELP1* exon 20 (**Fig. 6K**).

Measuring Hill coefficients, however, did not reveal statistically significant synergy at *SMN2* exon 7 for a branaplam/ASOi6 cocktail (**Fig. 6H**) or an ASOi6/ASOi7 cocktail (**Fig. 6J**). We suspected that this lack of statistically significant synergy could be due to the inherent difficulty of inferring precise Hill coefficient values from dose-response data. To test for synergy in a potentially more sensitive manner, we measured inclusion/exclusion ratios for drug mixtures that linearly interpolate between (100% drug 1, 0% drug 2) and (0% drug 1, 100% drug 2). We then assessed synergy based on whether any intermediate mixtures of these two drugs yielded higher inclusion/exclusion ratios than either drug alone. As expected, the results showed no synergy for risdiplam/branaplam mixtures (**Fig. 6L**). By contrast, strong synergy was observed for

risdiplam/ASOi6 mixtures (**Fig. 6M**), branaplam/ASOi6 mixtures (**Fig. 6N**), and ASOi6/ASOi7 mixtures (**Fig. 6O**). This finding confirms that the null results in **Figs. 6H,J** were due to a lack of statistical power, not a true lack of synergy. We conclude that synergy is widespread (and possibly universal) among splice-modifying drugs that can simultaneously promote inclusion of the same cassette exon.

Discussion

We have introduced a coarse-grained biophysical-modeling framework for splice-modifying drugs. We used this framework to analyze data from MPSAs, RNA-seq experiments, and precision dose-response curves. The results quantitatively define the 5'ss specificities of risdiplam and branaplam, and fundamentally change the mechanistic understanding of how these two small-molecule drugs function. Contrary to the prevailing two-site hypothesis for risdiplam[18,20], our results show that risdiplam does not function, even in part, by binding a purine tract within *SMN2* exon 7. The results also suggest that branaplam binds U1/5'ss complexes in two distinct interaction modes: one interaction mode that confers specificity similar to risdiplam, and a second interaction mode that confers alternative sequence specificity. The results further show—remarkably—that single-drug cooperativity and multi-drug synergy are widespread in the dose-response behavior of splice-modifying drugs. These findings establish our biophysical-modeling framework as a powerful tool in quantitative pharmacology, reveal new knowledge about the mechanisms of two clinically important drugs, and suggest new approaches for developing new splice-modifying therapeutics.

Our coarse-grained biophysical model for the 5'ss specificities of risdiplam and branaplam provide new mechanistic insight into how these two drugs interact with the U1/5'ss complex. The 5'ss specificities of risdiplam and branaplam are consistent with a bulge-repair mechanism[19], in that both drugs require a non-canonical $G_{-2}pA_{-1}$ dinucleotide in the target 5'ss. However, both risdiplam and branaplam exhibit additional specificity both upstream and downstream of the $G_{-2}pA_{-1}$ dinucleotide, specificity that is not obviously explained by existing structural data. The two interaction modes of branaplam suggested by our model further challenge the existing mechanistic understanding of how small-molecule splice-modifying drugs can function. More generally, our finding that two independently developed small-molecule therapeutics target the same non-canonical U1/5'ss complex, and not other RNA features, and that doing so confers an unexpectedly high level of specificity, underscores the importance of non-canonical 5' splice sites, such as those containing shifted registers or asymmetric bulges[79,80], as targets for future therapeutic development.

Our dose-response studies of individual splice-modifying drugs reveal that such drugs often exhibit cooperativity, i.e., have Hill coefficients greater than one. We describe this cooperativity as "anomalous" because it appears not to be due to multiple drug molecules simultaneously binding to the same RNA/protein complex. One possible explanation for the widespread anomalous cooperativity of splice-modifying drugs is the presence of biochemical feedback that couples the splicing of multiple pre-mRNA transcripts from the same gene. A second possible explanation for this widespread anomalous cooperativity is kinetic proofreading during the splicing of individual pre-mRNA transcripts[81], as kinetic proofreading could cause the binding of a drug to its target to be effectively "read out" by the spliceosome more than once. Additional quantitative studies will be needed to establish the roles, if any, that these two possible mechanisms play in sensitizing pre-mRNA transcripts to the effects of splice-modifying drugs.

Our dose-response studies with mixtures of splice-modifying drugs further reveal widespread synergy between drugs that are able to simultaneously stimulate inclusion of the same cassette exon. We expect that other alternative splicing processes, such as alternative 5'ss usage, alternative 3'ss usage, intron retention, and mutually exclusive cassette exons, might be affected by splice-modifying drugs in similar synergistic ways. Developing coarse-grained biophysical models that accurately predict this synergistic behavior is an important goal for future work, as it has the potential to provide mechanistic insight into the stages of spliceosome assembly and mRNA processing that splice-modifying drugs target, as well as guide the development of drug-cocktail therapies.

Our findings have immediate implications for the understanding and development of new splice-modifying therapies. First, our experimental and analytical approach can be used to define the specificities of other splice-modifying small molecules. Obvious candidates include kinetin[82], RECTAS[76], and BPN-15477[83], which have been developed as potential treatments for familial dysautonomia. Second, our two-interaction-mode

model for branaplam suggests that the specificity of branaplam for pseudoexon 50a in *HTT*[54,56,57] might be increased, and thus clinical side-effects decreased, by chemical changes that eliminate the risdiplam-like interaction mode. Third, our observation of widespread multi-drug synergy should motivate the clinical investigation of splice-modifying drug cocktails. We note that drug effects need to be large for this type of synergy to have a substantial effect on PSI. Drug cocktails that leverage this type of synergy are therefore likely to be most therapeutically useful for promoting mRNA isoforms that naturally occur at very low levels, (e.g., inclusion of pseudoexon 50a in *HTT*).

More generally, our work establishes the value of biophysical models in studies of splice-modifying drugs. Quantitative models based on statistical mechanics and chemical kinetics have, over the last century, played a central role in enzymology and the development of protein-targeted therapeutics[58–60]. The complexity of the spliceosome, however, has prevented the direct application of these models to splice-modifying drugs. Here we established the utility of biophysical models that coarse-grain out complex mechanistic details, but retain enough information to make useful predictions and illuminate molecular mechanisms. In particular, we showed how these models can be used to quantitatively synthesize data from multiple experimental modalities, including MPSAs and RNA-seq experiments. In addition to facilitating the development of new therapies, this biophysical-modeling strategy will likely facilitate the use of splice-modifying drugs in quantitative studies of the fundamental mechanisms of alternative mRNA splicing.

Materials and Methods: MPSA experiments used three independently constructed *SMN2* exon 7 minigene libraries, as well as previously described minigene libraries for *ELP1* exon 20[62]. Three biological replicates were performed for each MPSA library in each experimental condition. RNA-seq experiments were performed in HeLa cells using five biological replicates per condition. MPSA data was analyzed using custom Python scripts. RNA-seq data was analyzed using rMATS, followed by custom Python scripts. Bayesian model inference was carried out in STAN and in Python using numpyro. See **Supplemental Information** for details.

Data Availability: MPSA and RNA-seq data have been deposited in the NCBI GEO database (accession number GSE221868). Data-analysis scripts have been deposited on GitHub at https://github.com/jbkinney/22_drugs.

Author Contributions: MSW, YI, CM-G, ARK and JBK designed the research. ARK and JBK oversaw the research. YI, MSW, and AA performed the experiments. MK, CM-G, and JBK analyzed the data. SH performed the molecular dynamics simulations. JBK, YI, CM-G, and SH wrote the manuscript with additional contributions from MSW, AA, MK, DMM, and ARK.

Acknowledgements: We thank Christopher Trotta (PTC Therapeutics), Leemor Joshua-Tor (CSHL), and John Moses (CSHL) for helpful conversations. This work was supported by a JSPS Overseas Research Fellowship (YI), an Interdisciplinary Scholar in Experimental and Quantitative Biology fellowship from the Simons Center for Quantitative Biology at CSHL (MSW), the Simons Foundation (SH), NIH grant R35 GM133613 (CM-G, DMM), the Alfred P. Sloan foundation (DMM), NIH grant R37 GM42699 (YI, MSW, ARK), NIH grant R35 GM133777 (MSW, AA, JBK), NIH grant R01 HG011787 (MK, JBK), and additional funding from the Simons Center for Quantitative Biology at CSHL (DMM, JBK). Experiments were carried out using shared resources provided by the CSHL Cancer Center and supported by NIH grant P30 CA045508.

Competing Interests: ARK is: an inventor on issued nusinersen patents licensed by CSHL to Ionis Pharmaceuticals and Biogen; an inventor on an issued patent for familial dysautonomia ASOs; a co-founder, Director, Chair of the SAB, and shareholder of Stoke Pharmaceuticals; a paid consultant for Biogen; a collaborator of Ionis Pharmaceuticals; and a member of the SABs and shareholder of Skyhawk Pharmaceuticals, Envisagenics, and Autoimmunity BioSolutions.

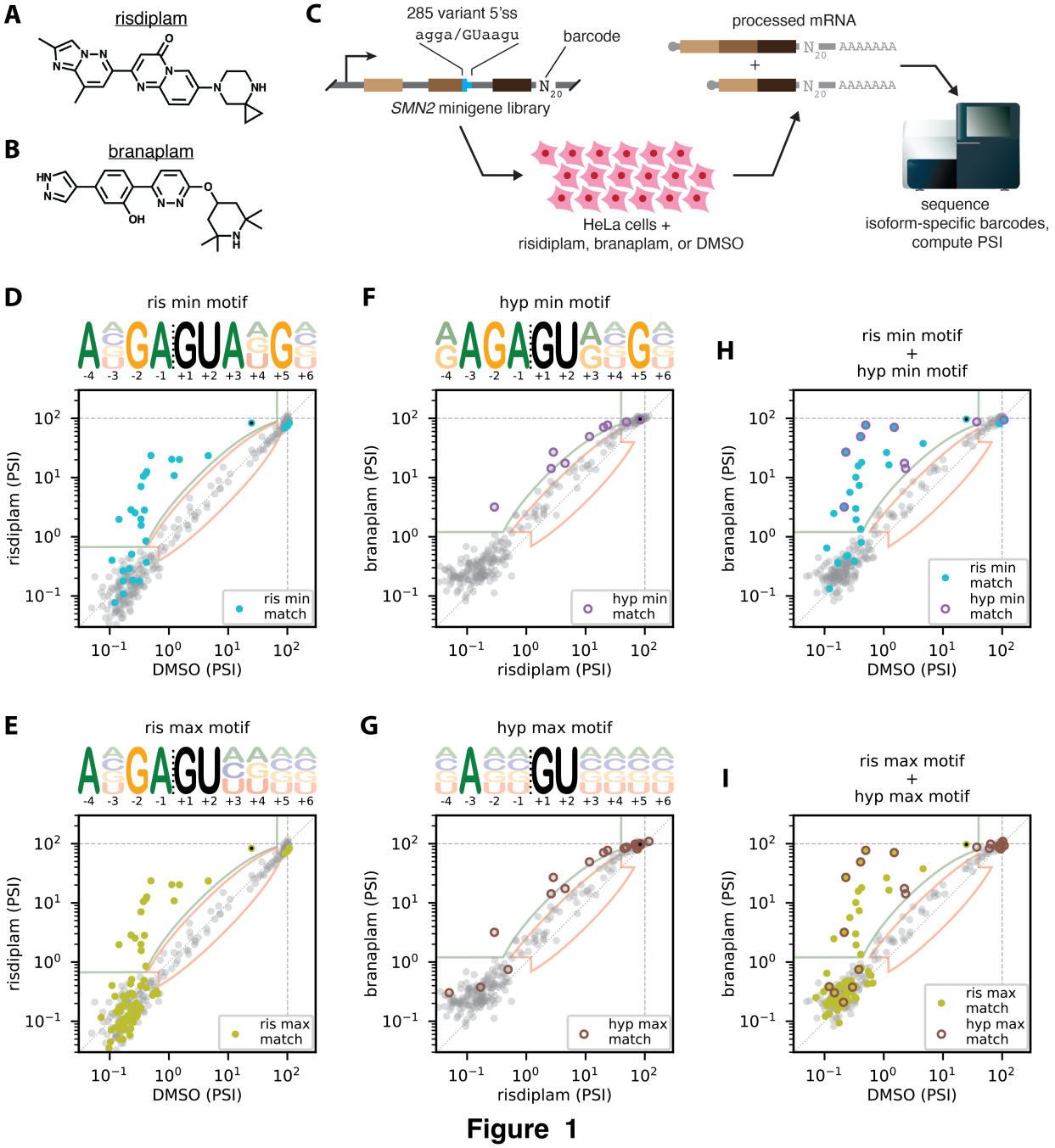

Figure 1

Figure 1. MPSAs define the 5'ss specificities of risdiplam and branaplam. (**A**) Risdiplam. (**B**) Branaplam. (**C**) MPSA performed on 285 variant 5'ss sequences in the context of an *SMN2* minigene comprising exons 6-8 and introns 6,7. (**D-I**) PSI values in the presence of risdiplam, branaplam, or DMSO, measured by MPSA. Results for (**D,E**) risdiplam vs. DMSO, (**F,G**) branaplam vs. risdiplam, and (**H,I**) branaplam vs DMSO. Colors indicate 5'ss that match the ris min motif (panel **D**; cyan dots), the ris max motif (panel **E**; mustard dots), the hyp min motif (panel **F**; blue circles), and the hyp max motif (panel **G**; brown circles). Light green outlined areas, 5'ss activated by y-axis treatment relative to x-axis treatment. Peach outlined areas, 5'ss insensitive to y-axis treatment relative to x-axis treatment. Black dot, wild-type *SMN2* exon 7 5'ss (AGGA/GUAAGU). MPSA, massively parallel splicing assay. 5'ss, 5' splice site. PSI, percent spliced in. DMSO, dimethyl sulfoxide.

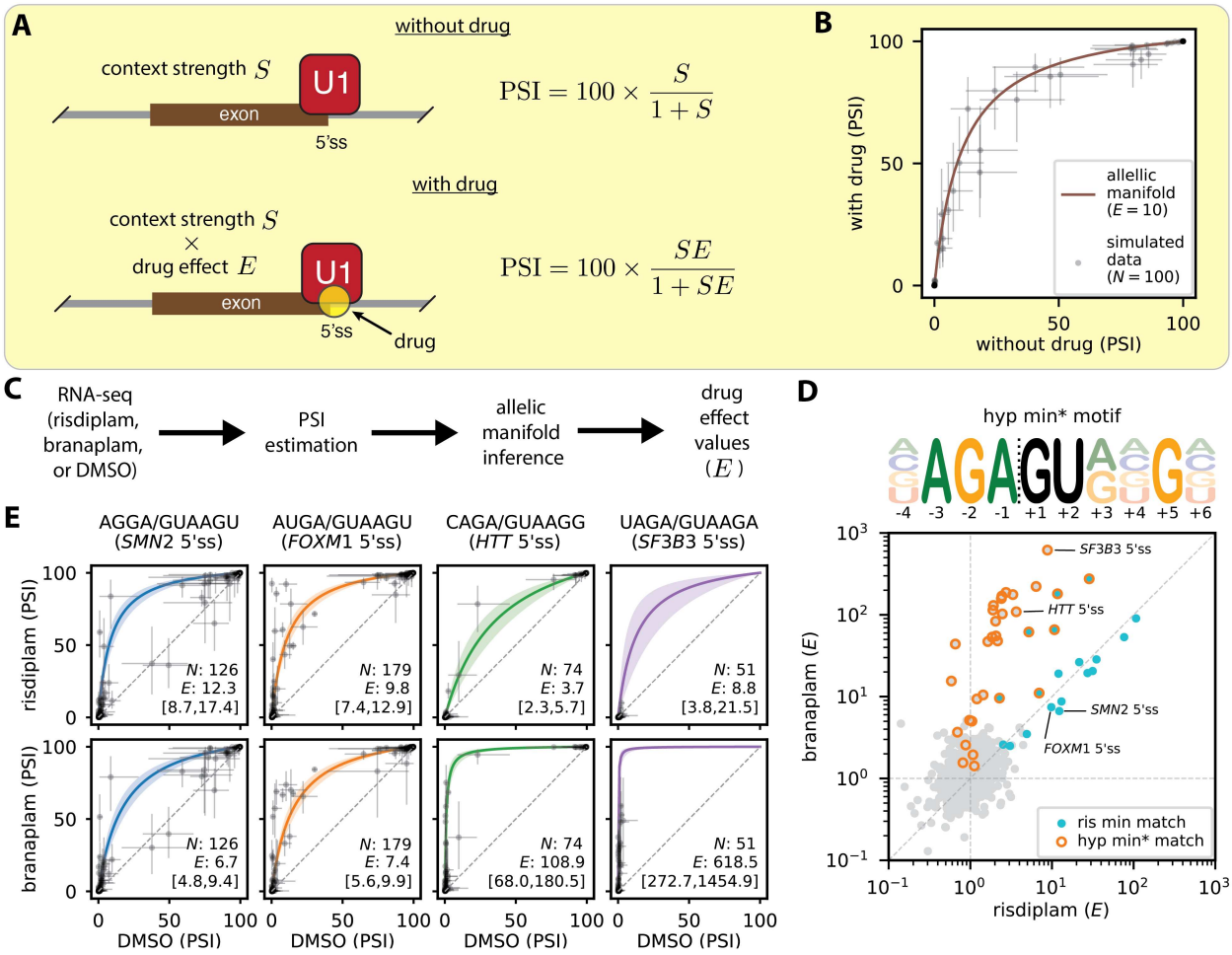

Figure 2

Figure 2. RNA-seq confirms and refines the specificities of risdiplam and branaplam. (**A**) Coarse-grained biophysical model for PSI as a function of 5'ss-specific drug effect (quantified by E) and locus-specific context strength (quantified by S). (**B**) Example allelic manifold and simulated RNA-seq data. (**C**) Experimental and analytical approach for defining 5'ss-specific drug effects from RNA-seq data. (**D**) Scatter plot of drug effects determined for 2,521 distinct 5'ss sequences, each occurring in at least 10 cassette exons throughout the transcriptome, together with a sequence logo visualization of the hyp min* IUPAC motif. Cyan dots, 5'ss sequences matching the ris min motif. Orange circles, 5'ss sequences matching the hyp min* motif. *SMN2* 5'ss: AGGA/GUAAGU, sequence of the 5'ss of *SMN2* exon 7. *FOXM1* 5'ss: AUGA/GUAAGU, sequence of the alternative 5'ss of *FOXM1* exon 9. *HTT* 5'ss: CAGA/GUAAGG, sequence of the 5'ss of *HTT* pseudoexon 50a. *SF3B3* 5'ss: UAGA/GUAAGA, sequence of the 5'ss of *SF3B3* pseudoexon 2a. (**E**) Allelic manifolds determined for the four 5'ss sequences annotated in panel **D**. N, number of exons having the indicated 5'ss and for which PSI was measured. E, 5'ss-dependent drug effect inferred by Bayesian curve fitting (median and 95% posterior credible interval). PSI, percent spliced in. 5'ss, 5' splice site. DMSO, dimethyl sulfoxide.

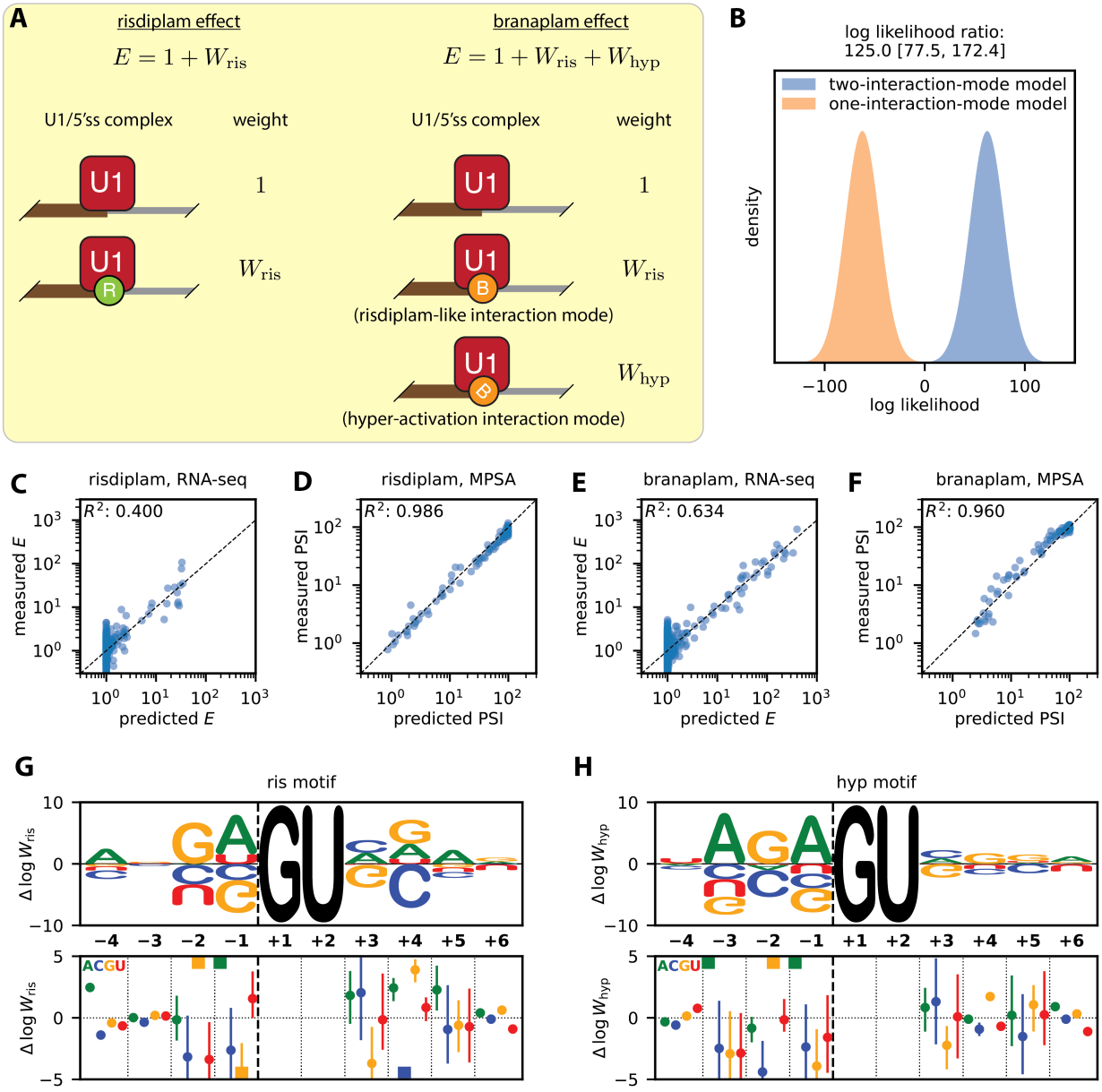

Figure 3

Figure 3. Coarse-grained biophysical modeling of risdiplam and branaplam specificity. (**A**) The "two-interaction-mode" biophysical model. Drug effect is determined by the U1/5'ss complexes that can occur in the presence of each drug. Each complex has a "weight": W_{ris} is the weight of complexes bound by risdiplam or bound by branaplam in the risdiplam-like interaction mode; W_{hyp} is the weight of the complex bound by branaplam in the hyper-activation interaction mode. W_{ris} and W_{hyp} are functions of 5'ss sequence. The parameters of W_{ris} comprise the "ris motif", and the parameters of W_{hyp} comprise the "hyp motif". See also **Fig. S9**. (**B**) Log likelihood values (centered about zero) for the two-interaction-mode model and for a competing one-interaction-mode model (**Fig. S10**). Distributions[84] show variation over Bayesian posterior samples of model parameters. Corresponding log likelihood ratios (median and 95% credible interval) are also shown. (**C-F**) Experimentally measured vs. model-predicted PSI values and drug-effect values. PSI values are from the *SMN2* exon 7 MPSA (**Fig. 1**); drug-effect values are from RNA-seq (**Fig. 2**). (**G,H**) Inferred additive parameters for (**G**) the ris motif and (**H**) the hyp motif. Top panels show median parameter values illustrated as sequence logos[85]. Bottom panels show medians (colored dots, with colors corresponding to each of the four RNA bases as indicated) and 95% credible intervals (colored lines) for motif parameters. Colored squares, median values that lie outside the y-axis limits. 5'ss, 5' splice site. MPSA, massively parallel splicing assay.

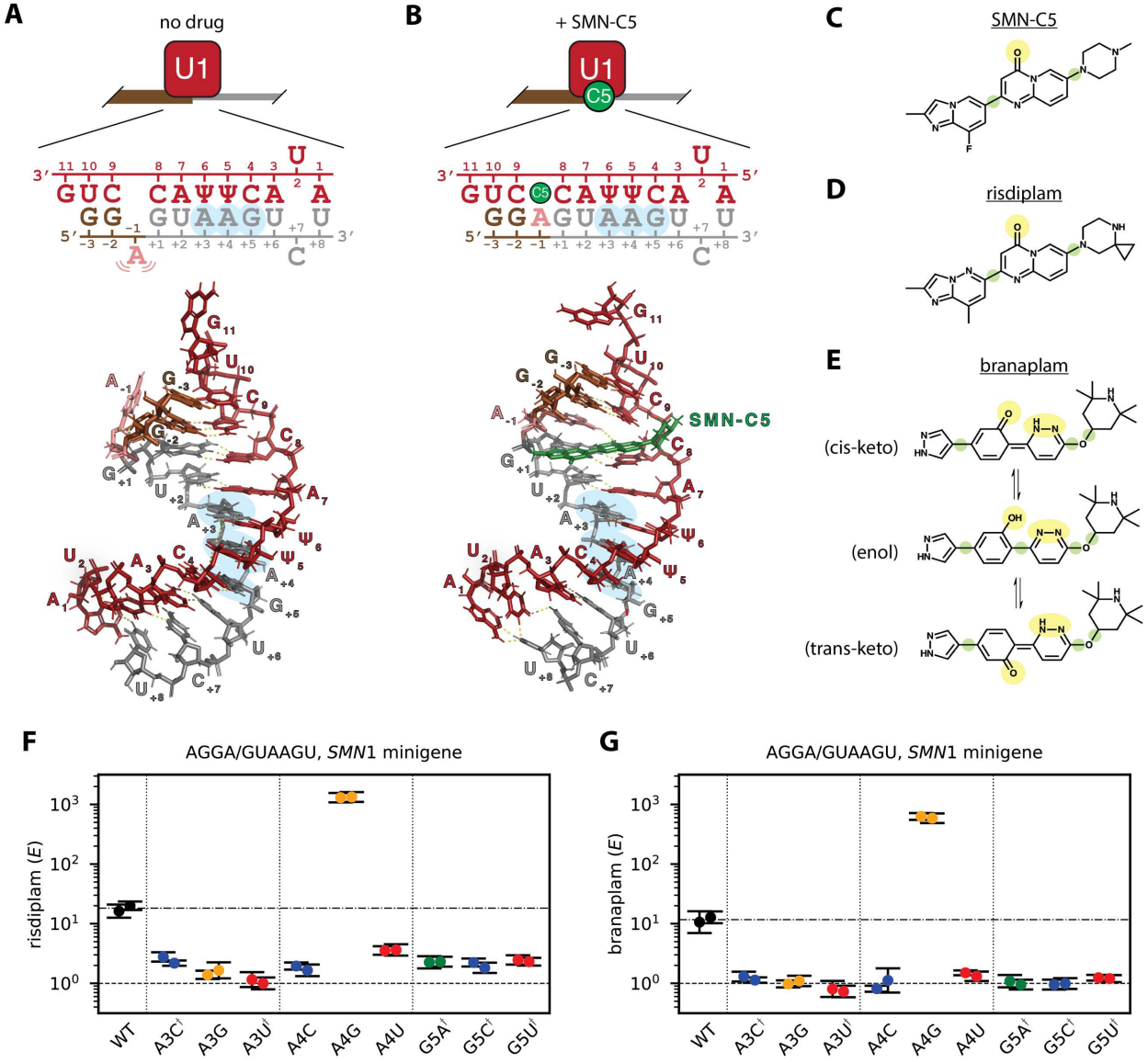

Figure 4

Figure 4. Risdiplam and branaplam specificities are incompletely explained by the bulge repair mechanism. (**A,B**) Bulge-repair mechanism proposed for the specificity of risdiplam. NMR structures (PDB:6HMI and PDB:6HMO, from ref.[19]) show U1-snRNA/5'ss complex in the (**A**) presence and (**B**) absence of SMN-C5, a risdiplam analog. A schematic of each structure is also shown. Red, U1 snRNA; brown, exonic 5'ss RNA; gray, intronic 5'ss RNA; green, SMN-C5; salmon, bulged A_{-1} stabilized by SMN-C5. Blue highlight, intronic positions observed to affect the activities of risdiplam and branaplam in panels **F** and **G**. (**C-E**) Planar structures of (**C**) SMN-C5, (**D**) risdiplam, and (**E**) three tautomeric forms of branaplam (cis-keto, trans-keto, and enol). Yellow highlight, potential hydrogen-bonding partners for the amino group of A_{-1}. Green highlight, rotational degree of freedom. (**F,G**) qPCR validation of intronic specificities for (**F**) risdiplam and (**G**) branaplam, assayed on single nucleotide variants of AGGA/GUAAGU in the context of an *SMN1* minigene. E denotes drug effect, which was measured by qPCR using $E = 2^{-\Delta C_t}$; note that $E = 1$ corresponds to no drug effect. Dots, biological replicates; error bars, standard error across technical replicates; dashed line, no effect; dashed/dotted line, wild-type effect value (geometric mean of biological replicates). Daggers indicate 5'ss variants for which the dominant inclusion isoform uses a cryptic 5'ss with +1 position at +52 of *SMN1* intron 7.

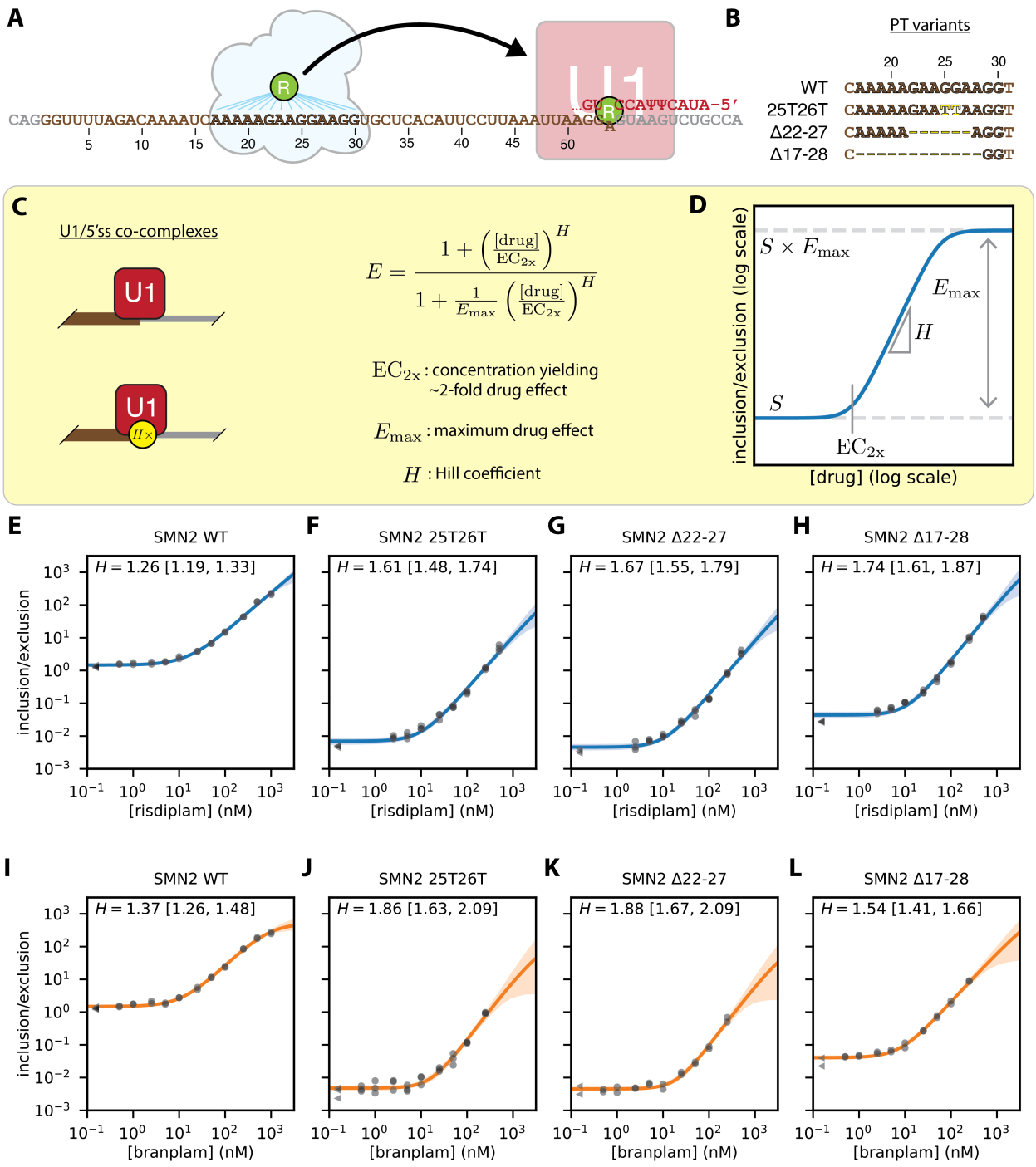

Figure 5

Figure 5. Dose-response curves falsify the two-site hypothesis for risdiplam. (**A**) Two-site hypothesis for risdiplam activity at *SMN2* exon 7. Cloud, proteins hypothesized to mediate the effect of risdiplam at the PT of *SMN2* exon 7 [hnRNP G (ref.[18]) or FUBP1 and KHSRP (ref.[20])]. (**B**) PT variants assayed in *SMN2* minigenes. (**C**) Biophysical model for concentration-dependent drug activity; see also **Fig. S14**. (**D**) Schematic illustration of model predictions for the inclusion/exclusion ratio as a function of drug concentration, as well as how model parameters shape this function. (**E-H**) Risdiplam titration curves for *SMN2* exon 7 minigenes containing (**E**) the wild-type PT or (**F-H**) mutated PTs. (**I-L**) Branaplam titration curves for *SMN2* exon 7 minigenes containing (**I**) the wild-type PT or (**J-L**) mutated PTs. Dots and triangles, qPCR data for biological replicates at nonzero drug concentration (dots) or zero drug concentration (triangles). Line and shaded region, predictions (median and

95% credible interval) of the inferred dose-response curve. H, inferred Hill coefficient (median and 95% credible interval). PT, purine tract.

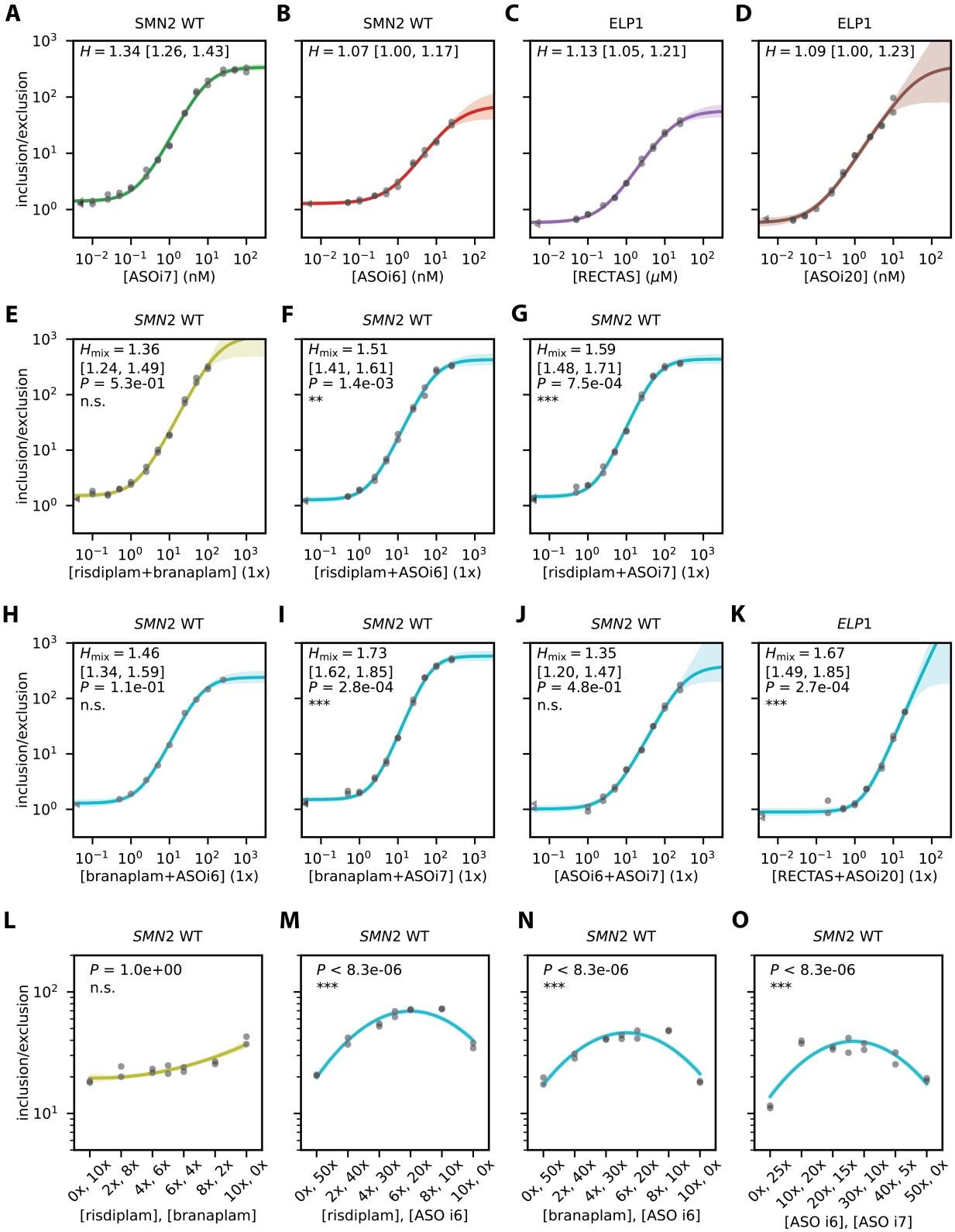

Figure 6

Figure 6. Anomalous cooperativity and multi-drug synergy among splice-modifying drugs. (**A,B**) Single-drug dose-response curves for *SMN2* exon 7 in response to (**A**) ASOi7 and (**B**) ASOi6. (**C,D**) Single-drug dose-response curves for *ELP* exon 20 in response to (**C**) RECTAS and (**D**) ASOi20. (**E-J**) Two-drug dose-response curves for *SMN2* exon 7 in response to (**E**) a risdiplam/branaplam cocktail, (**F**) a risdiplam/ASOi6

cocktail, (**G**) a risdiplam/ASOi7 cocktail, (**H**) a branaplam/ASOi6 cocktail, (**I**) a branaplam/ASOi7 cocktail, and (**J**) an ASOi6/ASOi7 cocktail. (**K**) Two-drug dose-response curve for *ELP1* exon 20 in response to a RECTAS/ASOi20 cocktail. A 1x cocktail corresponds to a mixture of 0.5x of each component drug, where a 1x concentration of each component drug (corresponding to approximate $\mathrm{EC}_{2\mathrm{x}}$ values) is 14 nM for risdiplam, 7 nM for branaplam, 0.1 nM for ASOi7, 0.6 nM for ASOi6, 300 nM for RECTAS, and 0.08 nM for ASOi20. H, single-drug Hill coefficient (median and 95% credible interval). H_{mix}, drug cocktail Hill coefficient (median and 95% credible interval). P, p-value for no-synergy null hypothesis (i.e., that H_{mix} is not larger than both $H_{\mathrm{drug}\,1}$ and $H_{\mathrm{drug}\,2}$). (**L-O**) Two-drug linear mixture curves measured for *SMN2* exon 7 in response to (**L**) risdiplam/branaplam mixtures, (**M**) risdiplam/ASOi6 mixtures, (**N**) branaplam/ASOi7 mixtures, and (**O**) ASOi6/ASOi7 mixtures. Inferred curves are second-order polynomials fit using a Bayesian inference procedure. P, p-value for no synergy null hypothesis (i.e., that the maximal inclusion/exclusion ratio occur at one of the two ends of the mixture curve). ***, $P < 0.001$; **, $P < 0.01$; *, $P < 0.05$; n.s., $P \geq 0.05$.

References

1. Tang, Z., Zhao, J., Pearson, Z. J., Boskovic, Z. V. & Wang, J. RNA-targeting splicing modifiers: drug development and screening assays. *Molecules* 26, 2263 (2021).

2. Warner, K. D., Hajdin, C. E. & Weeks, K. M. Principles for targeting RNA with drug-like small molecules. *Nat Rev Drug Discov* 17, 547–558 (2018).

3. Daguenet, E., Dujardin, G. & Valcárcel, J. The pathogenicity of splicing defects: mechanistic insights into pre-mRNA processing inform novel therapeutic approaches. *EMBO Rep* 16, 1640–1655 (2015).

4. Wu, P. Inhibition of RNA-binding proteins with small molecules. *Nat Rev Chem* 4, 441–458 (2020).

5. Scotti, M. M. & Swanson, M. S. RNA mis-splicing in disease. *Nat Rev Genet* 17, 19–32 (2015).

6. Ravi, B., Chan-Cortés, M. H. & Sumner, C. J. Gene-targeting therapeutics for neurological disease: lessons learned from spinal muscular atrophy. *Annu Rev Med* 72, 1–14 (2021).

7. Levin, A. A. Treating disease at the RNA level with oligonucleotides. *New Engl J Med* 380, 57–70 (2019).

8. Crooke, S. T., Baker, B. F., Crooke, R. M. & Liang, X. Antisense technology: an overview and prospectus. *Nat Rev Drug Discov* 20, 427–453 (2021).

9. Crooke, S. T., Witztum, J. L., Bennett, C. F. & Baker, B. F. RNA-targeted therapeutics. *Cell Metab* 27, 714–739 (2018).

10. Barraza, S. J., Bhattacharyya, A., Trotta, C. R. & Woll, M. G. Targeting strategies for modulating pre-mRNA splicing with small molecules: recent advances. *Drug Discov Today* 28, 103431 (2022).

11. Neil, C. R., Seiler, M. W., Reynolds, D. J., Smith, J. J., Vaillancourt, F. H., Smith, P. G. & Agrawal, A. A. Reprogramming RNA processing: an emerging therapeutic landscape. *Trends Pharmacol Sci* 43, 437–454 (2022).

12. Hua, Y., Vickers, T. A., Okunola, H. L., Bennett, C. F. & Krainer, A. R. Antisense masking of an hnRNP A1/A2 intronic splicing silencer corrects SMN2 splicing in transgenic mice. *Am J Hum Genet* 82, 834–848 (2008).

13. Finkel, R. S., Chiriboga, C. A., Vajsar, J., Day, J. W., Montes, J., Vivo, D. C. D., Yamashita, M., Rigo, F., Hung, G., Schneider, E., Norris, D. A., Xia, S., Bennett, C. F. & Bishop, K. M. Treatment of infantile-onset spinal muscular atrophy with nusinersen: a phase 2, open-label, dose-escalation study. *Lancet* 388, 3017–3026 (2016).

14. Bennett, C. F., Krainer, A. R. & Cleveland, D. W. Antisense oligonucleotide therapies for neurodegenerative diseases. *Annu Rev Neurosci* 42, 385–406 (2019).

15. Naryshkin, N. A., Weetall, M., Dakka, A., Narasimhan, J., Zhao, X., Feng, Z., Ling, K. K. Y., Karp, G. M., Qi, H., Woll, M. G., Chen, G., Zhang, N., Gabbeta, V., Vazirani, P., Bhattacharyya, A., Furia, B., Risher, N., Sheedy, J., Kong, R., Ma, J., Turpoff, A., Lee, C.-S., Zhang, X., Moon, Y.-C., Trifillis, P., Welch, E. M., Colacino, J. M., Babiak, J., Almstead, N. G., Peltz, S. W., Eng, L. A., Chen, K. S., Mull, J. L., Lynes, M. S., Rubin, L. L., Fontoura, P., Santarelli, L., Haehnke, D., McCarthy, K. D., Schmucki, R., Ebeling, M., Sivaramakrishnan, M., Ko, C.-P., Paushkin, S. V., Ratni, H., Gerlach, I., Ghosh, A. & Metzger, F. SMN2 splicing modifiers improve motor function and longevity in mice with spinal muscular atrophy. *Science* 345, 688–693 (2014).

16. Ratni, H., Ebeling, M., Baird, J., Bendels, S., Bylund, J., Chen, K. S., Denk, N., Feng, Z., Green, L., Guerard, M., Jablonski, P., Jacobsen, B., Khwaja, O., Kletzl, H., Ko, C.-P., Kustermann, S., Marquet, A., Metzger, F., Mueller, B., Naryshkin, N. A., Paushkin, S. V., Pinard, E., Poirier, A., Reutlinger, M., Weetall, M., Zeller, A., Zhao, X. & Mueller, L. Discovery of risdiplam, a selective survival of motor neuron-2 (SMN2) gene splicing modifier for the treatment of spinal muscular atrophy (SMA). *J Med Chem* 61, 6501–6517 (2018).

17. Dhillon, S. Risdiplam: first approval. *Drugs* 80, 1853–1858 (2020).

18. Sivaramakrishnan, M., McCarthy, K. D., Campagne, S., Huber, S., Meier, S., Augustin, A., Heckel, T., Meistermann, H., Hug, M. N., Birrer, P., Moursy, A., Khawaja, S., Schmucki, R., Berntenis, N., Giroud, N., Golling, S., Tzouros, M., Banfai, B., Duran-Pacheco, G., Lamerz, J., Liu, Y. H., Luebbers, T., Ratni, H., Ebeling, M., Cléry, A., Paushkin, S., Krainer, A. R., Allain, F. H.-T. & Metzger, F. Binding to SMN2 pre-mRNA-protein complex elicits specificity for small molecule splicing modifiers. *Nat Commun* 8, 1476 (2017).

19. Campagne, S., Boigner, S., Rüdisser, S., Moursy, A., Gillioz, L., Knörlein, A., Hall, J., Ratni, H., Cléry, A. & Allain, F. H.-T. Structural basis of a small molecule targeting RNA for a specific splicing correction. *Nat Chem Biol* 1, 919–8 (2019).

20. Wang, J., Schultz, P. G. & Johnson, K. A. Mechanistic studies of a small-molecule modulator of SMN2 splicing. *Proc Natl Acad Sci USA* 115, 201800260 (2018).

21. Ratni, H., Scalco, R. S. & Stephan, A. H. Risdiplam, the first approved small molecule splicing modifier drug as a blueprint for future transformative medicines. *ACS Med Chem Lett* 12, 874–877 (2021).

22. Ratni, H., Mueller, L. & Ebeling, M. Rewriting the (tran)script: application to spinal muscular atrophy. *Progr Med Chem* 58, 119–156 (2019).

23. Tang, Z., Akhter, S., Ramprasad, A., Wang, X., Reibarkh, M., Wang, J., Aryal, S., Thota, S. S., Zhao, J., Douglas, J. T., Gao, P., Holmstrom, E. D., Miao, Y. & Wang, J. Recognition of single-stranded nucleic acids by small-molecule splicing modulators. *Nucleic Acids Res* 49, 7870–7883 (2021).

24. Singh, R. N., Ottesen, E. W. & Singh, N. N. The first orally deliverable small molecule for the treatment of spinal muscular atrophy. *Neurosci Insights* 15, 1–11 (2020).

25. Monteys, A. M., Hundley, A. A., Ranum, P. T., Tecedor, L., Muehlmatt, A., Lim, E., Lukashev, D., Sivasankaran, R. & Davidson, B. L. Regulated control of gene therapies by drug-induced splicing. *Nature* 596, 291–295 (2021).

26. Taladriz-Sender, A., Campbell, E. & Burley, G. A. Splice-switching small molecules: A new therapeutic approach to modulate gene expression. *Methods* 167, 134–142 (2019).

27. Markati, T., Fisher, G., Ramdas, S. & Servais, L. Risdiplam: an investigational survival motor neuron 2 (SMN2) splicing modifier for spinal muscular atrophy (SMA). *Expert Opin Inv Drug* 31, 451–461 (2022).

28. Costales, M. G., Childs-Disney, J. L., Haniff, H. S. & Disney, M. D. How we think about targeting RNA with small molecules. *J Med Chem* 63, 8880–8900 (2020).

29. Centa, J. L. & Hastings, M. L. Alternative splicing, methods and protocols. *Methods Mol Biol* 2537, 21–36 (2022).

30. Lejman, J., Zieliński, G., Gawda, P. & Lejman, M. Alternative splicing role in new therapies of spinal muscular atrophy. *Genes* 12, 1346 (2021).

31. Bush, J. A., Williams, C. C., Meyer, S. M., Tong, Y., Haniff, H. S., Childs-Disney, J. L. & Disney, M. D. Systematically studying the effect of small molecules interacting with RNA in cellular and preclinical models. *ACS Chem Biol* 16, 1111–1127 (2021).

32. Kelaini, S., Chan, C., Cornelius, V. A. & Margariti, A. RNA-binding proteins hold key roles in function, dysfunction, and disease. *Biology* 10, 366 (2021).

33. Ando, S., Suzuki, S., Okubo, S., Ohuchi, K., Takahashi, K., Nakamura, S., Shimazawa, M., Fuji, K. & Hara, H. Discovery of a CNS penetrant small molecule SMN2 splicing modulator with improved tolerability for spinal muscular atrophy. *Sci Rep* 10, 17472 (2020).

34. Meyer, S. M., Williams, C. C., Akahori, Y., Tanaka, T., Aikawa, H., Tong, Y., Childs-Disney, J. L. & Disney, M. D. Small molecule recognition of disease-relevant RNA structures. *Chem Soc Rev* 49, 7167–7199 (2020).

35. Angelbello, A. J., Chen, J. L. & Disney, M. D. Small molecule targeting of RNA structures in neurological disorders. *Ann NY Acad Sci* 1471, 57–71 (2020).

36. Zhu, S., Rooney, S. & Michlewski, G. RNA-targeted therapies and high-throughput screening methods. *Int J Mol Sci* 21, 2996 (2020).

37. Morgan, B. S., Sanaba, B. G., Donlic, A., Karloff, D. B., Forte, J. E., Zhang, Y. & Hargrove, A. E. R-BIND: an interactive database for exploring and developing RNA-targeted chemical probes. *ACS Chem Biol* 14, 2691–2700 (2019).

38. Black, A. J., Gamarra, J. R. & Giudice, J. More than a messenger: Alternative splicing as a therapeutic target. *BBA-Gene Regul Mech* 1862, 194395 (2019).

39. Mercuri, E., Sumner, C. J., Muntoni, F., Darras, B. T. & Finkel, R. S. Spinal muscular atrophy. *Nat Rev Dis Primers* 8, 52 (2022).

40. Giorgio, A. D. & Duca, M. Synthetic small-molecule RNA ligands: future prospects as therapeutic agents. *Med Chem Commun* 10, 1242–1255 (2019).

41. Debaize, L. & Troadec, M.-B. The master regulator FUBP1: its emerging role in normal cell function and malignant development. *Cell Mol Life Sci* 76, 259–281 (2019).

42. Donlic, A. & Hargrove, A. E. Targeting RNA in mammalian systems with small molecules. *Wiley Interdiscip Rev RNA* 9, e1477 (2018).

43. Messina, S. & Sframeli, M. New treatments in spinal muscular atrophy: positive results and new challenges. *J Clin Med* 9, 2222 (2020).

44. Yu, A.-M., Choi, Y. H. & Tu, M.-J. RNA drugs and RNA targets for small molecules: principles, progress, and challenges. *Pharmacol Rev* 72, 862–898 (2020).

45. Ojala, K. S., Reedich, E. J., DiDonato, C. J. & Meriney, S. D. In search of a cure: the development of therapeutics to alter the progression of spinal muscular atrophy. *Brain Sci* 11, 194 (2021).

46. Marabti, E. E. & Abdel-Wahab, O. Therapeutic modulation of RNA splicing in malignant and non-malignant disease. *Trends Mol Med* 27, 643–659 (2021).

47. Chaytow, H., Faller, K. M. E., Huang, Y.-T. & Gillingwater, T. H. Spinal muscular atrophy: from approved therapies to future therapeutic targets for personalized medicine. *Cell Rep Med* 2, 100346 (2021).

48. Malard, F., Mackereth, C. D. & Campagne, S. Principles and correction of 5'-splice site selection. *RNA Biol* 19, 943–960 (2022).

49. Vincent, F., Nueda, A., Lee, J., Schenone, M., Prunotto, M. & Mercola, M. Phenotypic drug discovery: recent successes, lessons learned and new directions. *Nat Rev Drug Discov* 1–16 (2022). doi:10.1038/s41573-022-00472-w

50. Singh, N. N., O'Leary, C. A., Eich, T., Moss, W. N. & Singh, R. N. Structural context of a critical exon of spinal muscular atrophy gene. *Frontiers Mol Biosci* 9, 928581 (2022).

51. Palacino, J., Swalley, S. E., Song, C., Cheung, A. K., Shu, L., Zhang, X., Hoosear, M. V., Shin, Y., Chin, D. N., Keller, C. G., Beibel, M., Renaud, N. A., Smith, T. M., Salcius, M., Shi, X., Hild, M., Servais, R., Jain, M., Deng, L., Bullock, C., McLellan, M., Schuierer, S., Murphy, L., Blommers, M. J. J., Blaustein, C., Berenshteyn, F., Lacoste, A., Thomas, J. R., Roma, G., Michaud, G. A., Tseng, B. S., Porter, J. A., Myer, V. E., Tallarico, J. A., Hamann, L. G., Curtis, D., Fishman, M. C., Dietrich, W. F., Dales, N. A. & Sivasankaran, R. SMN2 splice modulators enhance U1-pre-mRNA association and rescue SMA mice. *Nat Chem Biol* 11, 511–517 (2015).

52. Cheung, A. K., Hurley, B., Kerrigan, R., Shu, L., Chin, D. N., Shen, Y., O'Brien, G., Sung, M. J., Hou, Y., Axford, J., Cody, E., Sun, R., Fazal, A., Fridrich, C., Sanchez, C. C., Tomlinson, R. C., Jain, M., Deng, L., Hoffmaster, K., Song, C., Hoosear, M. V., Shin, Y., Servais, R., Towler, C., Hild, M., Curtis, D., Dietrich, W. F., Hamann, L. G., Briner, K., Chen, K. S., Kobayashi, D., Sivasankaran, R. & Dales, N. A. Discovery of small molecule splicing modulators of survival motor neuron-2 (SMN2) for the treatment of spinal muscular atrophy. *J Med Chem* 61, 11021–11036 (2018).

53. Figueiredo, M. Novartis stopping work on branaplam as oral SMA therapy. *SMA News Today* (2021). at <https://smanewstoday.com/news/novartis-stopping-development-branaplam-sma-oral-therapy/>

54. Bhattacharyya, A., Trotta, C. R., Narasimhan, J., Wiedinger, K. J., Li, W., Effenberger, K. A., Woll, M. G., Jani, M. B., Risher, N., Yeh, S., Cheng, Y., Sydorenko, N., Moon, Y.-C., Karp, G. M., Weetall, M., Dakka, A., Gabbeta, V., Naryshkin, N. A., Graci, J. D., Tripodi, T., Southwell, A., Hayden, M., Colacino, J. M. & Peltz, S. W. Small molecule splicing modifiers with systemic HTT-lowering activity. *Nat Commun* 12, 7299 (2021).

55. Novartis. Novartis receives FDA fast track designation for branaplam (LMI070) for the treatment of Huntington's disease. (2021). at <https://www.novartis.com/news/novartis-receives-fda-fast-track-designation-branaplam-lmi070-treatment-huntingtons-disease>

56. Keller, C. G., Shin, Y., Monteys, A. M., Renaud, N., Beibel, M., Teider, N., Peters, T., Faller, T., St-Cyr, S., Knehr, J., Roma, G., Reyes, A., Hild, M., Lukashev, D., Theil, D., Dales, N., Cha, J.-H., Borowsky, B., Dolmetsch, R., Davidson, B. L. & Sivasankaran, R. An orally available, brain penetrant, small molecule lowers huntingtin levels by enhancing pseudoexon inclusion. *Nat Commun* 13, 1150 (2022).

57. Krach, F., Stemick, J., Boerstler, T., Weiss, A., Lingos, I., Reischl, S., Meixner, H., Ploetz, S., Farrell, M., Hehr, U., Kohl, Z., Winner, B. & Winkler, J. An alternative splicing modulator decreases mutant HTT and improves the molecular fingerprint in Huntington's disease patient neurons. *Nat Commun* 13, 6797 (2022).

58. Gesztelyi, R., Zsuga, J., Kemeny-Beke, A., Varga, B., Juhasz, B. & Tosaki, A. The Hill equation and the origin of quantitative pharmacology. *Arch Hist Exact Sci* 66, 427–438 (2012).

59. Johnson, K. A. & Goody, R. S. The original Michaelis constant: translation of the 1913 Michaelis-Menten paper. *Biochemistry* 50, 8264–8269 (2011).

60. Segel, I. H. *Enzyme Kinetics*. (Wiley-Interscience, 1975).

61. Baeza-Centurion, P., Miñana, B., Schmiedel, J. M., Valcárcel, J. & Lehner, B. Combinatorial genetics reveals a scaling law for the effects of mutations on splicing. *Cell* 176, 549-563.e23 (2019).

62. Wong, M. S., Kinney, J. B. & Krainer, A. R. Quantitative activity profile and context dependence of all human 5' splice sites. *Mol Cell* 71, 1012-1026.e3 (2018).

63. Cornish-Bowden, A. Nomenclature for incompletely specified bases in nucleic acid sequences: recommendations. *Nucleic Acids Res* 13, 3021–3030 (1985).

64. Kinney, J. B. & McCandlish, D. M. Massively parallel assays and quantitative sequence-function relationships. *Annu Rev Genom Hum G* 20, 99–127 (2019).

65. Shea, M. A. & Ackers, G. K. The OR control system of bacteriophage lambda: a physical-chemical model for gene regulation. *J Mol Biol* 181, 211–230 (1985).

66. Bintu, L., Buchler, N. E., Garcia, H. G., Gerland, U., Hwa, T., Kondev, J. & Phillips, R. Transcriptional regulation by the numbers: models. *Curr Opin Genet Dev* 15, 116–124 (2005).

67. Kuhlman, T., Zhang, Z., Saier, M. H. & Hwa, T. Combinatorial transcriptional control of the lactose operon of Escherichia coli. *Proc Natl Acad Sci USA* 104, 6043–6048 (2007).

68. Kinney, J. B., Murugan, A., Callan, C. G. & Cox, E. C. Using deep sequencing to characterize the biophysical mechanism of a transcriptional regulatory sequence. *Proc Natl Acad Sci USA* 107, 9158–9163 (2010).

69. Phillips, R., Kondev, J., Theriot, J. & Garcia, H. *Physical Biology of the Cell*. (Garland Science, 2012).

70. Wong, F. & Gunawardena, J. Gene Regulation in and out of Equilibrium. *Annu Rev Biophys* 49, 199–226 (2020).

71. Forcier, T. L., Ayaz, A., Gill, M. S., Jones, D., Phillips, R. & Kinney, J. B. Measuring cis-regulatory energetics in living cells using allelic manifolds. *eLife* 7, e40618 (2018).

72. Singh, N. N., Androphy, E. J. & Singh, R. N. In vivo selection reveals combinatorial controls that define a critical exon in the spinal muscular atrophy genes. *RNA* 10, 1291–1305 (2004).

73. Hofmann, Y., Lorson, C. L., Stamm, S., Androphy, E. J. & Wirth, B. Htra2-β1 stimulates an exonic splicing enhancer and can restore full-length SMN expression to survival motor neuron 2 (SMN2). *Proc Natl Acad Sci USA* 97, 9618–9623 (2000).

74. Wu, X., Wang, S.-H., Sun, J., Krainer, A. R., Hua, Y. & Prior, T. W. A-44G transition in SMN2 intron 6 protects patients with spinal muscular atrophy. *Hum Mol Genet* 26, 2768–2780 (2017).

75. Ajiro, M., Awaya, T., Kim, Y. J., Iida, K., Denawa, M., Tanaka, N., Kurosawa, R., Matsushima, S., Shibata, S., Sakamoto, T., Studer, R., Krainer, A. R. & Hagiwara, M. Therapeutic manipulation of IKBKAP mis-splicing with a small molecule to cure familial dysautonomia. *Nat Commun* 12, 4507 (2021).

76. Yoshida, M., Kataoka, N., Miyauchi, K., Ohe, K., Iida, K., Yoshida, S., Nojima, T., Okuno, Y., Onogi, H., Usui, T., Takeuchi, A., Hosoya, T., Suzuki, T. & Hagiwara, M. Rectifier of aberrant mRNA splicing recovers tRNA modification in familial dysautonomia. *Proc Natl Acad Sci USA* 112, 2764–2769 (2015).

77. Sinha, R., Kim, Y. J., Nomakuchi, T., Sahashi, K., Hua, Y., Rigo, F., Bennett, C. F. & Krainer, A. R. Antisense oligonucleotides correct the familial dysautonomia splicing defect in IKBKAP transgenic mice. *Nucleic Acids Res* 46, 4833–4844 (2018).

78. Greco, W. R., Bravo, G. & Parsons, J. C. The search for synergy: a critical review from a response surface perspective. *Pharmacol Rev* 47, 331–85 (1995).

79. Roca, X., Akerman, M., Gaus, H., Berdeja, A., Bennett, C. F. & Krainer, A. R. Widespread recognition of 5' splice sites by noncanonical base-pairing to U1 snRNA involving bulged nucleotides. *Gene Dev* 26, 1098–1109 (2012).

80. Roca, X. & Krainer, A. R. Recognition of atypical 5' splice sites by shifted base-pairing to U1 snRNA. *Nat Struct Mol Biol* 16, 176–182 (2009).

81. Semlow, D. R. & Staley, J. P. Staying on message: ensuring fidelity in pre-mRNA splicing. *Trends Biochem Sci* 37, 263–273 (2012).

82. Slaugenhaupt, S. A., Mull, J., Leyne, M., Cuajungco, M. P., Gill, S. P., Hims, M. M., Quintero, F., Axelrod, F. B. & Gusella, J. F. Rescue of a human mRNA splicing defect by the plant cytokinin kinetin. *Hum Mol Genet* 13, 429–436 (2004).

83. Gao, D., Morini, E., Salani, M., Krauson, A. J., Chekuri, A., Sharma, N., Ragavendran, A., Erdin, S., Logan, E. M., Li, W., Dakka, A., Narasimhan, J., Zhao, X., Naryshkin, N., Trotta, C. R., Effenberger, K. A., Woll, M. G., Gabbeta, V., Karp, G., Yu, Y., Johnson, G., Paquette, W. D., Cutting, G. R., Talkowski, M. E. & Slaugenhaupt, S. A. A deep learning approach to identify gene targets of a therapeutic for human splicing disorders. *Nat Commun* 12, 3332 (2021).

84. Chen, W.-C., Tareen, A. & Kinney, J. B. Density estimation on small data sets. *Phys Rev Lett* 121, 160605 (2018).

85. Tareen, A. & Kinney, J. B. Logomaker: beautiful sequence logos in Python. *Bioinformatics* 36, 2272–2274 (2020).